Octahedral vs Trigonal Prismatic Geometry in a Series of Catechol Macrobicyclic Ligand-Metal Complexes

Timothy B. Karpishin, T. D. P. Stack, and Kenneth N. Raymond*

Contribution from the Department of Chemistry, University of California, Berkeley, California 94720. *Received June 29, 1992*

Abstract: A series of metal complexes of the macrobicyclic tris(catecholate) ligand bicapped(TRENCAM), BCT, has been prepared and crystallographically characterized to investigate the stabilization of trigonal prismatic geometry in these complexes: $[Al^{III}(BCT)]^{3-}$, $[Ti^{IV}(BCT)]^{2-}$, $[V^{IV}(BCT)]^{2-}$, $[Fe^{III}(BCT)]^{3-}$, and $[Ga^{III}(BCT)]^{3-}$. Although crystal field stabilization energy plays no role in any of these metal-ligand complexes, the stereochemistries vary significantly between pseudotrigonal prismatic and pseudooctahedral. Spectroscopic data indicate that π-bonding stabilizes the pseudotrigonal prismatic geometry in the case of the d-block metal complexes. Two Fe^{III} complexes of other members of this family of ligands have been structurally characterized for comparative purposes: $[Fe^{III}(BCTPT)]^{3-}$ and $[Fe(eta)_3]^{3-}$, where BCTPT is the macrobicyclic ligand bicapped(TPTCAM) and eta is the bidentate ligand *N,N'*-diethylterephthalamide. The structure of the free ligand, $H_6(BCT)$ is also presented. Crystal data: space group, a, b, c, α, β, γ, V, Z (only undefined cell parameters are listed): $K_3[Al(BCT)]\cdot 6acetone\cdot 2H_2O$: $P2_12_12_1$, 13.170 (3) Å, 21.362 (4) Å, 22.516 (4) Å, 6335 (4) Å^3, 4; $K_2[Ti(BCT)]\cdot 6DMF\cdot 2H_2O$: $P\bar{1}$, 11.878 (2) Å, 12.151 (3) Å, 26.033 (5) Å, 81.02 (2)°, 85.14 (1)°, 61.24 (2)°, 3253 (1) Å^3, 2; $K_2[V(BCT)]\cdot 4DMF\cdot 1.5H_2O$: $P\bar{1}$, 12.930 (4) Å, 16.065 (5) Å, 16.049 (4) Å, 91.22 (2)°, 111.67 (2)°, 112.62 (3)°, 2807 (4) Å^3, 2; $K_3[Fe(BCT)]\cdot 6DMF\cdot H_2O$: $P2_1/c$, 17.039 (6) Å, 16.347 (6) Å, 24.138 (4) Å, 102.00 (3)°, 6576 (5) Å^3, 4; $K_3[Ga(BCT)]\cdot 6DMF\cdot H_2O$: $Pbca$, 16.816 (6) Å, 23.889 (5) Å, 33.154 (7) Å, 13319 (10) Å^3, 8; $K_3[Fe(BCTPT)]\cdot 4DMF\cdot 0.5H_2O$: $P2_1/n$, 12.018 (2) Å, 22.187 (7) Å, 24.187 (6) Å, 92.96 (2)°, 6441 (5) Å^3, 4; $K_3[Fe(eta)_3]\cdot 3acetone\cdot 2ethanol$: $R3c$ (hex), 14.529 (3) Å, 52.021 (12) Å, 9511 (7) Å^3, 6; $H_6(BCT)\cdot H_2O$: $P2_1/n$, 15.374 (3) Å, 14.328 (2) Å, 17.044 (2) Å, 108.44 (1)°, 3562 (2) Å^3, 4.

Introduction

Although examples of trigonal prismatic geometry have long been known for solid-state materials such as MoS_2,[1] six-coordinate molecular complexes are usually octahedral.[2] Ligand-ligand repulsion is greater in a trigonal prismatic (TP) complex (relative to O_h), and thus it is only in special cases where TP geometry is observed. Several tris(dithiolate) complexes are trigonal prismatic, such as $[Mo(S_2C_6H_4)_3]$[3] and $[Re(S_2C_2Ph_2)_3]$.[4] It has been proposed that interligand S-S bonding may be responsible for the TP geometries in these complexes; however, this is still unresolved.[5] The TP geometry recently found for $[Zr(Me)_6]^{2-}$[6] has been explained by theoretical studies[7] which have suggested that for such d^0 complexes the molecular orbital stabilization is sufficient to overcome the increased ligand-ligand repulsion energy.

In addition to electronic factors, observed trigonal prismatic geometries can be attributed to the constraints of the ligand. Holm and co-workers, for example, have prepared a macrobicyclic ligand which, by virtue of its rigidity and small cavity, results in near-TP geometry for Ni^{II}, Co^{II}, and Zn^{II}.[8] In other cases, where there appears to be no better rationale for the observed trigonal prismatic geometry, crystal packing forces have been invoked.[5]

The recent observation that the complex Na_3[Fe(bicapped-TRENCAM] (see Figure 1) is prefectly trigonal prismatic[9] was surprising for several reasons: (1) This structure represents the only example of TP geometry for Fe^{III}. The smallest twist angle, α (Figure 2), previously determined for a Fe^{III} complex was 25.2° in the structure of [Fe(TCTA)] (TCTA = 1,4,7-triazacyclononane-*N,N',N''*-triacetate).[10] (2) The structures of several tris(catecholate) metal complexes are known, including $[Fe^{III}(catechol)_3]^{3-}$, and all have been found to be pseudooctahedral (i.e., $\alpha > 40°$).[11] (3) There are very few TP complexes with six coordinating oxygens; considerable deviations from O_h in six-coordinate complexes have occurred primarily with sulfur ligands.[12]

The initial rationalization for the observed TP geometry in Na_3[Fe(bicappedTRENCAM)] was based on the hydrogen bonding between the amide hydrogens and the catecholate oxygens of the ligand.[9,13] In the structure the three arms of the macrobicycle are planar, resulting in six strong hydrogen bonds. The stabilization due to these H-bonds, in addition to the lack of crystal field stabilization energy (CFSE) in high-spin Fe^{III}, provided a plausible explanation for this rare coordination geometry.

The potential for CFSE in trigonal prismatic and octahedral geometries is illustrated with the d-orbital splitting diagram in Figure 3.[14,15] For no d-orbital configuration is the TP geometry favored. High-spin Fe^{III} (d^5) should show no electronic preference for either of the limiting geometries, since the destabilization of the e^a orbitals is exactly compensated by the stabilization of the e^b orbitals. Neither is there a preference in the case of V^{IV} (d^1), since the d_{z^2} (a_1) orbital does not change in energy (within the approximation that the angle between the M-O bond and the trigonal axis does not change significantly). There are however configurations (e.g., d^3, low-spin d^6) for which O_h geometry is strongly favored.

To probe the factors that result in the prismatic geometry of Na_3[Fe(bicapped-TRENCAM)], a series of metal complexes with the bicappedTRENCAM (BCT) ligand have been prepared and their structures determined. For each of the metal ions in this series, CFSE should have no effect on the geometries: Al^{III} (d^0), Ti^{IV} (d^0), V^{IV} (d^1), and Ga^{III} (d^{10}). Substantial differences in the

* Author to whom correspondence should be addressed.

(1) Dickinson, R. G.; Pauling, L. *J. Am. Chem. Soc.* **1923**, *45*, 1466.
(2) Kepert, D. L. In *Inorganic Stereochemistry*; Springer-Verlag: Berlin, 1982; p 92.
(3) Bennett, M. J.; Cowie, M.; Martin, J. L.; Takats, J. *J. Am. Chem. Soc.* **1973**, *95*, 7504.
(4) Stiefel, E. I.; Eisenberg. R.; Rosenberg, R. C.; Gray, H. B. *J. Am. Chem. Soc.* **1966**, *88*, 2956.
(5) Kepert, D. L. *Prog. Inorg. Chem.* **1977**, *23*, 1.
(6) Morse, P. M.; Girolami, G. S. *J. Am. Chem. Soc.* **1989**, *111*, 4114.
(7) Kang, S. K.; Albright. T. A.; Eisenstein, O. *Inorg. Chem.* **1989**, *28*, 1611.
(8) Larsen, E.; La Mar, G. N.; Wagner, B. E.; Parks, J. E.; Holm, R. H. *Inorg. Chem.* **1972**, *11*, 2652.
(9) McMurry, T. J.; Hosseini, M. W.; Garrett, T. M.; Hahn, F. E.; Reyes, Z. E.; Raymond, K. N. *J. Am. Chem. Soc.* **1987**, *109*, 7196.
(10) Wieghardt, K.; Bossek, U.; Chaudhuri, P.; Herrmann, W.; Menke, B. C.; Weiss, J. *Inorg. Chem.* **1982**, *21*, 4308.
(11) Borgias, B. A.; Barclay, S. J.; Raymond, K. N. *J. Coord. Chem.* **1986**, *15*, 109 and references therin.
(12) For an example of TP geometry with six oxygen ligands: Pierpont, C. G.; Buchanan, R. M. *J. Am. Chem. Soc.* **1975**, *97*, 4912.
(13) Garrett, T. M.; McMurry, T. J.; Hosseini, M. W.; Reyes, Z. E.; Hahn, F. E.; Raymond, K. N. *J. Am. Chem. Soc.* **1991**, *113*, 2965.
(14) This diagram was generated using crystal field theory, starting with the coordinates of a perfect octahedron and simply decreasing the twist angle, α, to arrive at TP geometry (ref 15).
(15) Companion, A. L.; Komarynsky, M. A. *J. Chem. Ed.* **1964**, *41*, 257.

0002-7863/93/1515-182$04.00/0

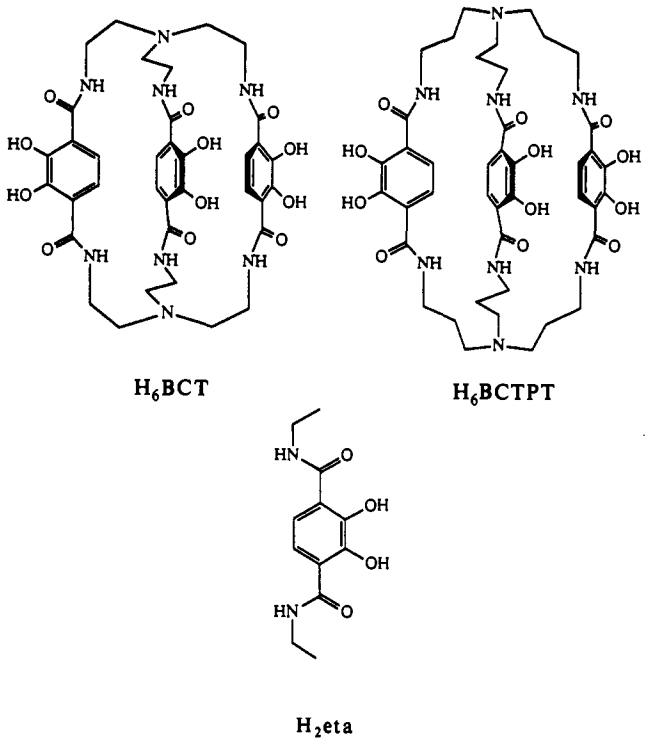

Figure 1. Ligands used in this study: bicappedTRENCAM, H_6BCT; bicappedTPTCAM, H_6BCTPT; *N,N'*-diethylterephthalamide, H_2eta.

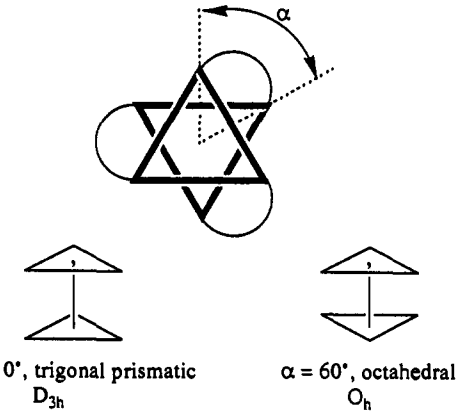

Figure 2. Definition of the trigonal twist angle, α, for tris(bidentate) metal complexes.

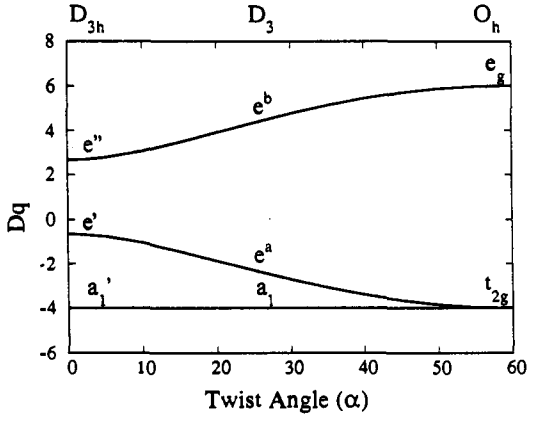

Figure 3. A d-orbital ligand field energy diagram for octahedral and trigonal prismatic geometries (the polar θ angles of the O atoms are fixed at 54.74°).

geometries of these metal–ligand complexes are found however, and these are discussed. In addition, a second structure of the $[Fe^{III}(BCT)]^{3-}$ anion (with K^+ cations rather than Na^+) has been determined; it shows some significant differences from the perfectly prismatic sodium salt. Two other Fe^{III} crystal structures are also presented which allow an evaluation of the steric requirements of the BCT ligand. One complex contains a similar macrobicyclic ligand that possesses a larger cavity: bicappedTPTCAM (Figure 1). The other is the sterically unconstrained $[Fe^{III}(eta)_3]^{3-}$ complex (Figure 1) which demonstrates the "relaxed" structure with these binding groups. The structure of the free ligand, $H_6(BCT)$, is also presented. Finally, comparisons are made of the electronic spectra of these complexes to rationalize the geometric differences in these tris(catecholate) metal complexes.

Scheme I

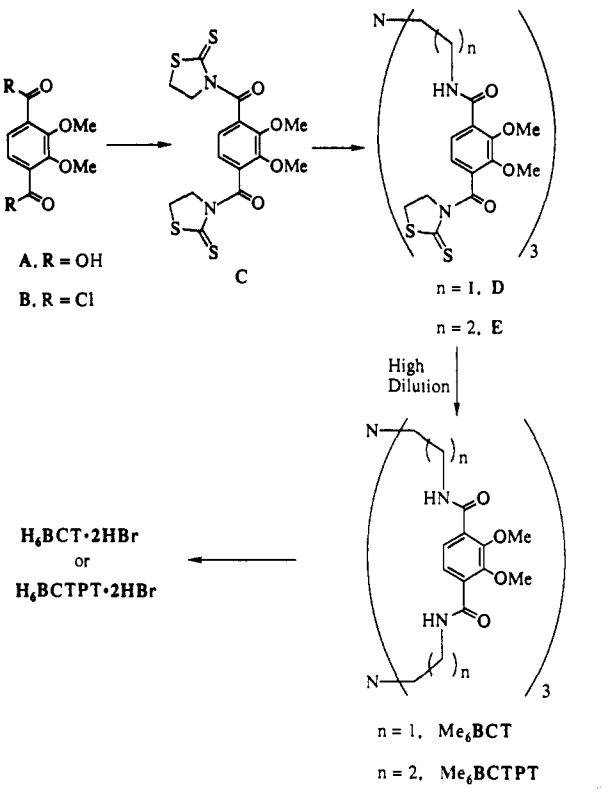

Results and Discussion

I. Ligand Syntheses. The syntheses of the macrobicyclic ligands bicappedTRENCAM (H_6BCT) and bicappedTPTCAM (H_6BCTPT) are outlined in Scheme I. Both ligands have been previously synthesized by a stepwise methodology.[13,16] A more direct route is presented here which represents significant improvements over those published procedures, in which two steps are removed from the syntheses, and the overall yields are approximately tripled. The starting material is 2,3-dimethoxyterephthalic acid[17] (**A** in Scheme I) which is prepared on a 100-g scale. The key to the improved syntheses lies in the use of 2,3-dimethoxyterephthalic acid bis(2-mercaptothiazolide) (**C**)—a robust crystalline material easily prepared in large scale from **A** via the acyl chloride (**B**) in ≈70% yield. The reactivity of 2-mercaptothiazolides is much lower than acyl chlorides or succinimide esters, allowing for the direct preparation of the monocapped precursors **D** and **E** (Scheme I) by reaction of tripodal amine (TREN or TPT) with a large excess of **C**. This reaction yields **D** in 67% yield and **E** in 75% yield *without* significant polymer formation, and the excess **C** can be easily recovered. In addition to the facile synthesis of **D** and **E**, coupling the amines with the 2-mercaptothiazolide group results in *much* higher yields in the final reaction. In the previous procedures, when the tripodal tris(acyl chloride) was coupled to

(16) McMurry, T. J.; Rodgers, S. J.; Raymond, K. N. *J. Am. Chem. Soc.* **1987**, *109*, 3451.
(17) Weitl, F. L.; Raymond, K. N.; Durbin, P. W. *J. Med. Chem.* **1981**, *24*, 203.

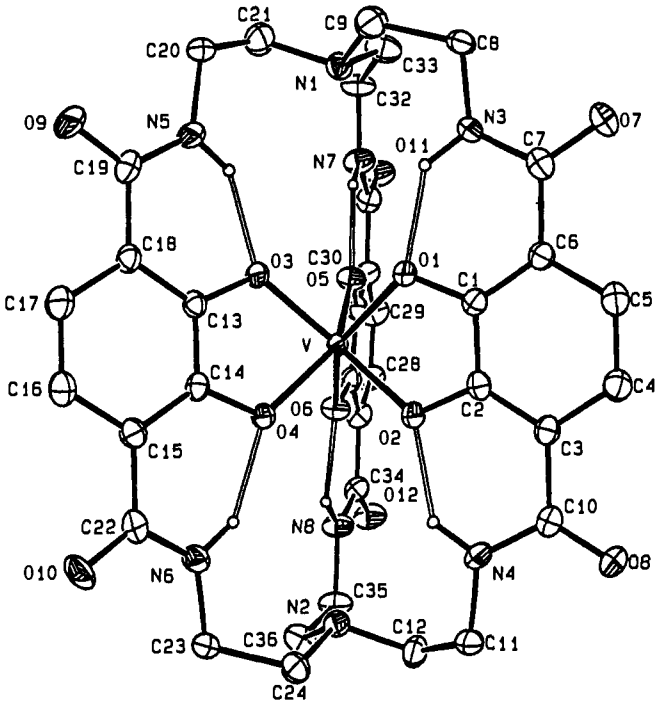

Figure 4. An ORTEP view of $[V(BCT)]^{2-}$.

TREN or TPT in a high dilution reaction, the yields of the methyl protected macrobicyclic compounds were 27% and 12%, respectively.[13,16] Using **D** and **E** to couple to TREN and TPT gives Me_6BCT and Me_6BCTPT in 65% and 39% yields, respectively. This remarkable improvement in yield in the high dilution reactions results from the lower reactivity of the 2-mercaptothiazolide group with primary amines. Deprotection of the methyl protected compounds with BBr_3 affords the ligands as their HBr salts.

II. Metal Complex Syntheses. The metal complexes are all synthesized anaerobically in ligand exchange reactions with the appropriate acetylacetonate starting material: $Al(acac)_3$, $[TiO(acac)_2]_2$, $VO(acac)_2$, $Fe(acac)_3$, or $Ga(acac)_3$. These reactions proceed immediately upon the addition of KOH. Column purification (Sephadex LH-20, in MeOH) then results in analytically pure metal complexes.

III. Comparisons of the Metal Complexes. In all, six metal complexes with the bicappedTRENCAM (BCT) ligand have now been structurally characterized. The structure of $Na_3[Fe^{III}(BCT)]$ has been communicated earlier,[9,13] here we present the structures of $K_3[Al^{III}(BCT)]$, $K_2[Ti^{IV}(BCT)]$, $K_2[V^{IV}(BCT)]$, $K_3[Fe^{III}(BCT)]$, and $K_3[Ga^{III}(BCT)]$. In addition, we have determined crystal structures of $K_3[Fe^{III}(BCTPT)]$, which has a larger metal cavity, and the unconstrained trisbidentate complex $K_3[Fe^{III}(eta)_3]$. An ORTEP view of the $[V(BCT)]^{2-}$ complex anion is shown in Figure 4. All of the BCT complexes show similar gross structural features, thus for comparative purposes, only the metal tris(catecholate) portion of each of the BCT structures is shown in Figure 5 as viewed down the pseudo 3-fold axes. Figure 5 also shows the tris(catecholate) portions of $[Fe(BCTPT)]^{3-}$ and $[Fe(eta)_3]^{3-}$.

For each of the metal ions in these complexes, there is no geometric preference dictated by d-electron stabilization. Therefore all of the BCT structures might be expected to adopt a geometry that is due solely to energetic stabilization of the *ligand*. In previous structural studies of a sexadentate ligand with metal ions that possess similar or no CFSE, the geometric differences have been shown to be minimal.[8,18] Substantial geometric differences, however, *do* exist among the series of BCT complexes. Selected structural data are presented in Table I.

The geometry of each BCT complex is classified most easily from the twist angles as shown in Figure 5. The twist angle divides

(18) Comba, P.; Sargeson, A. M.; Engelhardt, L. M.; Harrowfield, J. M.; White, A. H.; Horn, E.; Snow, M. R. *Inorg. Chem.* **1985**, *15*, 2325.

Table I. Selected Structural Data for the Metal Complexes

compound	twist angle (deg)	M–O (Å)	O–C (Å)	O–M–O (deg)	normalized bite[a]
$K_3[Al(BCT)]$	40.3	1.89	1.32	83.1	1.327
$K_2[Ti(BCT)]$	8.1	1.95	1.34	78.6	1.267
$K_2[V(BCT)]$	11.2	1.92	1.33	79.0	1.272
$K_3[Fe(BCT)]$	10.4	1.99	1.32	78.7	1.268
$Na_3[Fe(BCT)]$[b]	0.0	2.01	1.33	77.8	1.256
$K_3[Ga(BCT)]$	34.2	1.95	1.32	81.6	1.307
$K_3[Fe(BCTPT)]$	39.5	2.01	1.33	79.6	1.280
$K_3[Fe(eta)_3]$	40.0	2.03	1.32	79.1	1.274

compound	out of catechol plane[c] M (Å)	out of catechol plane[c] O's[d] (Å)	O–M–O vs catechol[e] (deg)	apical N–N (Å)
$K_3[Al(BCT)]$	0.05	0.20, −0.18	9.0	9.68
$K_2[Ti(BCT)]$	0.24	0.07, −0.05	10.3	9.87
$K_2[V(BCT)]$	0.19	0.04, −0.07	7.5	9.77
$K_3[Fe(BCT)]$	0.24	0.08, −0.07	9.4	9.76
$Na_3[Fe(BCT)]$[b]	0.82	0.01, 0.01	30.9	10.03
$K_3[Ga(BCT)]$	0.03	0.20, −0.20	9.3	9.69
$K_3[Fe(BCTPT)]$	0.15	0.008, 0.008	7.8	10.70
$K_3[Fe(eta)_3]$	0.003	0.01, −0.03	3.0	

[a] Normalized bite: $2\sin(\theta/2)$, where θ = O–M–O angle. [b] From ref 9. [c] Average distance of metal or ligating oxygens from catechol (C_6) plane. [d] One side of the plane is arbitrarily chosen as positive. [e] Average dihedral angle between O–M–O plane and catechol (C_6) plane.

Table II. Hydrogen Bonding Data for the Metal Complexes

compound	NCO vs catechol[a] (deg)	O···H[b] (Å)	O–H–N (deg)
$K_3[Al(BCT)]$	9.7	1.77	136.4
$K_2[Ti(BCT)]$	5.4	1.83	135.5
$K_2[V(BCT)]$	6.7	1.81	135.8
$K_3[Fe(BCT)]$	3.8	1.73	138.2
$Na_3[Fe(BCT)]$[c]	9.4	1.80	135.9
$K_3[Ga(BCT)]$	8.3	1.74	136.8
$K_3[Fe(BCTPT)]$	7.8	1.81	135.6
$K_3[Fe(eta)_3]$	10.0	1.79	132.6

[a] Dihedral angle between amide plane (NCO) and catechol (C_6) plane. [b] Calculated with an idealized N–H distance of 1.09 Å, ref 40. [c] From ref 9.

the complexes into two groups: pseudo-O_h (Al and Ga) and pseudo-TP (Ti, V, Fe). A finer geometrical classification results from the positioning of the metal and ligating catechol oxygens relative to the catechol (C_6) plane. In the pseudo-O_h complexes ($\alpha > 34°$) the metal sits in the plane of each catechol (C_6) ring, with each of the oxygen atoms nearly symmetrically positioned ≈0.2 Å above and below the plane for each of the three catecholate binding groups (Table I). In contrast, the oxygens in the Ti, V, and Fe complexes (where $\alpha < 11°$) are positioned *in* the plane of the catechol ring with the metal displaced *out* of the plane. An extreme is found in the Na^+ salt of the Fe complex where the Fe is displaced 0.82 Å out of the plane. This structural effect in $Na_3[Fe(BCT)]$ is also manifest in the dihedral angle between the O–M–O plane and the catechol plane, which is 30.9° (in the other BCT complexes that dihedral angle only varies slightly from 7–10°). These structures suggest that, as the twist angle decreases, the metal is forced out of the catechol plane, possibly because the cavity of the macrobicyclic ligand becomes too confining. The most stable (or "relaxed") geometry for these tris(terephthalamide) complexes is illustrated by $[Fe(eta)_3]^{3-}$, where the Fe *and* O atoms are positioned in the plane of the catechol ring and the twist angle is 40.0°. The $[Fe(BCTPT)]^{3-}$ complex is exceptional since the twist angle, 39.5°, results in a pseudo-O_h classification, but the coordination environment more closely resembles a TP complex with the Fe displaced 0.15 Å.

IV. Hydrogen Bonding. The initial reason given for the observed TP geometry in $Na_3[Fe(BCT)]$ was that the H-bonding from the amide H's to the catecholate oxygens stabilizes the structure.[9] In fact, this H-bonding is a prevalent feature of *all* the BCT structures (Figure 4). Metrical parameters relevant to

Table III. Summary of Crystallographic Data

compound	K_3[Al(BCT)]·6acetone·2H_2O	K_2[Ti(BCT)]·6DMF·2H_2O	K_2[V(BCT)]·4DMF·1.5H_2O	K_3[Fe(BCT)]·6DMF·H_2O	K_3[Ga(BCT)]·6DMF·H_2O	K_3[Fe(BCTPT)]·4DMF·0.5H_2O	K_3[Fe(eta)$_3$]·3acetone·2ethanol	H_6(BCT)·H_2O
formula	$AlK_3O_{20}N_8C_{54}H_{76}$	$TiK_2O_{20}N_{14}C_{54}H_{82}$	$VK_2O_{17.5}N_{12}C_{48}H_{67}$	$FeK_3O_{19}N_{14}C_{54}H_8$	$GaK_3O_{19}N_{14}C_{54}H_{80}$	$FeK_3O_{16.5}N_{12}C_{54}H_{29}$	$FeK_3O_{17}N_6C_{49}H_{72}$	$O_{13}N_8C_{36}H_{44}$
formula wt	1301.54	1373.44	1221.28	1402.48	1416.35	1283.04	1190.28	796.80
temp (K)	156	168	172	160	152	176	190	175
crystal system	orthorhombic	triclinic	triclinic	monoclinic	orthorhombic	monoclinic	rhombohedral	monoclinic
space group	$P2_12_12_1$ (no. 19)	$P\bar{1}$ (no 2)	$P\bar{1}$ (no. 2)	$P2_1/c$ (no. 14)	*Pbca* (no. 61)	$P2_1/n$ (no. 14)	*R3c* (no 161; hexagonal)	$P2_1/n$ (no. 14)
a(Å)	13.170 (3)	11.878 (2)	12.930 (4)	17.039 (6)	16.816 (6)	12.018 (2)	14.529 (3)	15.374 (3)
b(Å)	21.362 (4)	12.151 (3)	16.065 (5)	16.347 (6)	23.889 (5)	22.187 (7)		14.328 (2)
c(Å)	22.516 (4)	26.033 (5)	16.049 (4)	24.138 (4)	33.154 (7)	24.187 (6)	52.021 (12)	17.044 (2)
α(deg)		81.02 (2)	91.22 (2)					
β(deg)		85.14 (1)	111.67 (2)	102.00 (3)		92.96 (2)		108.44 (1)
γ(deg)		61.24 (2)	112.62 (3)					
Z	4	2	2	4	8	4	6	4
V (Å^3)	6335 (4)	3253 (1)	2807 (4)	6576 (5)	13319 (10)	6441 (5)	9511 (7)	3562 (2)
μ_{calc} (cm^{-1})	3.0	3.35	3.96	4.94	6.73	4.96	4.954	1.07
d_{calc} (d_{meas}) (g·cm^{-1})	1.36	1.402	1.454	1.416	1.413	1.331	1.25	1.486 (1.48)
F(000)	2744	1448	1288	2948	5936	2624	3762	1680
crystal size (mm)	0.13 × 0.32 × 0.26	0.34 × 0.31 × 0.39	0.28 × 0.50 × 0.60	0.15 × 0.15 × 0.40	0.30 × 0.40 × 0.50	0.50 × 0.40 × 0.35	0.30 × 0.20 × 0.15	0.22 × 0.20 × 0.15
radiation	Mo Kα	Mo Kα	Mo Kα	Mo Kα	Mo Kα	Mo Kα	Mo Kα	Mo Kα
h,*k*,*l* range	0 → 15, 0 → 25, 0 → 26	0 → 7, −13 → 13, −27 → 27	0 → 15, −19 → 19, −19 → 19	0 → 18, 0 → 17, −25 → 25	0 → 18, 0 → 25, 0 → 35	0 → 12, 0 → 23, −26 → 26	−15 → 15, −15 → 15, −57 → 57; cond: $-h+k+l = 3n$	0 → 16, 0 → 15, −18 → 18
2θ range	3.0–50.0	3.0–45.0	3.0–50.0	3.0–45.0	3.0–45.0	3.0–45.0	3.0–45.0	3.0–45.0
scan type	θ–2θ	ω	ω	θ–2θ	ω	θ–2θ	θ–2θ	θ–2θ
scan speed (deg/min)	4.1	4.1	5.5	4.1	4.1	4.1	4.0	4.1
reflcns collected	6160	5848	9859	9291	9479	9150	6328	5085
unique reflcns	6128	5848	9859	8560	8671	8391	2775	4656
data: ($F_o^2 > 3\sigma(F_o^2)$)	2662	4135	7016	4165	4677	4642	1174	1962
no. of params	378	814	792	817	781	771	84	514
data/param ratio	7.0	5.1	8.9	5.1	6.0	6.0	14.0	3.8
R	0.076	0.078	0.058	0.066	0.066	0.077	0.071	0.059
R_w	0.089	0.102	0.071	0.067	0.070	0.090	0.074	0.062
GOF	1.600	2.929	2.602	1.972	2.230	2.233	2.084	1.375

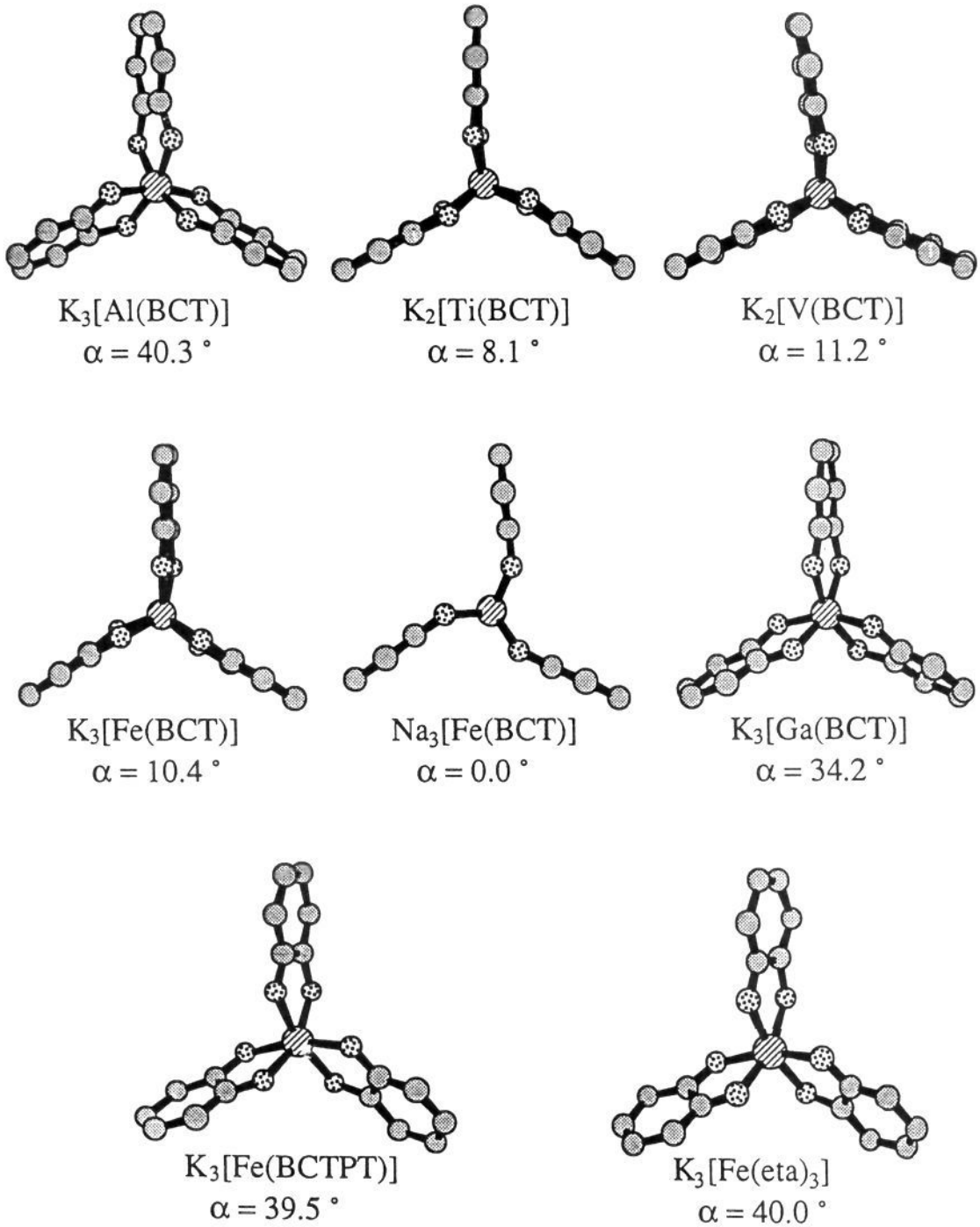

Figure 5. Diagram of the tris(catecholate) portions of the metal complexes in this study as viewed down the pseudo 3-fold axes.

the H-bonding are presented in Table II. A prior, a dihedral angle of 0° between the plane of the amide group (NCO) and the catechol ring would be anticipated to assure the strongest hydrogen bond. However angles in the range of 4–10° are consistently found in the bicapped structures (Table II) and in other tris(terephthalamide) structures.[19,20] In addition, crystal structures of the methylated forms of terephthalamide ligands display similar H-bonding patterns, and similar interplanar angles are observed.[21] These structural results are consistent with steric crowding of the amide hydrogens; i.e., the planes are slightly rotated to avoid steric congestion. The data in Table II show that strong H-bonding is maintained throughout the TP and pseudo-O_h complexes; there is no relation between the H-bonding and the observed twist angles.

V. Repulsion Energy Considerations. Since CFSE does not contribute to the observed differences in twist angle among the metal complexes examined, we can first analyze this situation in terms of simple repulsion energies. For idealized six-coordinate tris(bidentate) complexes, the stereochemistry is completely defined by the twist angle, α, and the normalized bite of the bidentate ligand.[2] The normalized bite, b, is defined as the distance between the coordinating atoms of the same bidentate ligand, divided by the M–L bond length. As the normalized bite of a bidentate ligand decreases, the optimum twist angle based on the lowest repulsive energy between the ligating atoms in the M(bidentate)$_3$ complex

(19) Stack, T. D. P.; Karpishin, T. B.; Raymond, K. N. *J. Am. Chem. Soc.* **1992**, *114*, 1512.
(20) Dewey, T. M.; Raymond, K. N., to be submitted for publication.
(21) Garrett, T. M.; Cass, M. E.; Raymond, K. N. *J. Coord. Chem.* **1992**, *25*, 241.

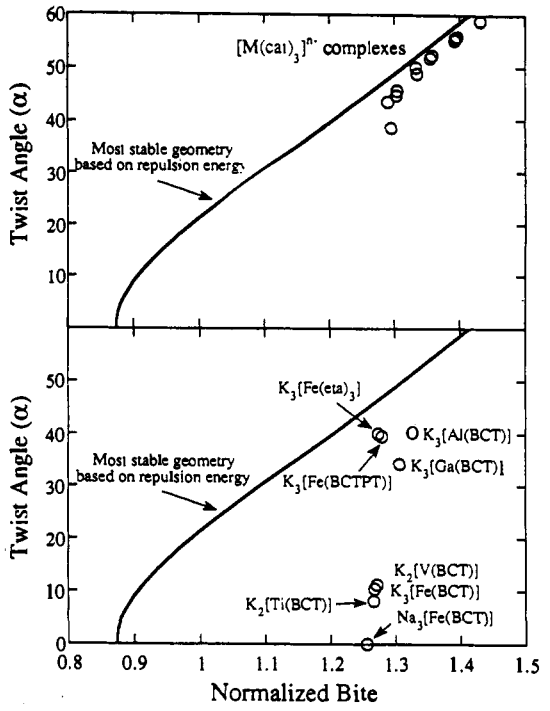

Figure 6. Plot of the observed twist angles vs the normalized bites. The line in the top and bottom portions represents the calculated optimum geometry; (top) 12 previously characterized tris(catecholate) metal complexes[11] and (bottom) the metal complexes in this study.

also decreases. This trend is shown by the theoretical line in the top and bottom portions of Figure 6, which was calculated using the method of Kepert.[2] The top portion of Figure 6 shows a plot of the observed twist angles vs the normalized bites for 12 crystallographically characterized tris(catecholate) metal complexes including Fe^{III}, V^{IV}, Ti^{IV}, and Ga^{III}.[11] In all these cases the complexes fall below the theoretical line. This positioning suggests that the optimum twist angle for unconstrained tris(catecholate) complexes is 3–5° below the theoretical value. The bottom portion of Figure 6 shows the corresponding plot for the structures presented here. Considering the location of $[Fe(eta)_3]^{3-}$ and the tris(catecholate) complexes on the plot, $[Al(BCT)]^{3-}$ and $[Ga(BCT)]^{3-}$ in addition to $[Fe(BCTPT)]^{3-}$ adopt geometries that seem to be dictated to a large extent by ligand–ligand repulsion. In contrast, the Ti, V, and Fe BCT complexes adopt geometries which cannot be attributed solely to steric repulsion; other factors must lead to the differences between the two groups of BCT complexes: (Ti, V, Fe) and (Al, Ga).

VI. Charge and Size Considerations. One factor which varies over the series of complexes is the size of the metal cation: Al^{III} = 0.54, Ti^{IV} = 0.61, V^{IV} = 0.58, Fe^{III} = 0.65, and Ga^{III} = 0.62 Å.[22] The size dramatically affects the M–O bond lengths in a systematic fashion (Table I); however, it does not correlate with the twist angles. In addition, although the charges on the complexes vary between (2–) and (3–), no obvious trends emerge. The most remarkable difference in twist angle is found in the Fe^{III} and Ga^{III} structures; the two metal ions are usually considered to be highly analogous because of similar size, charge, and physical properties.[11] Clearly an additional phenomenon is reponsible within the d-block metal complexes that, given the constraints of the BCT ligand, stabilizes their geometries close to TP.

VII. Electronic Absorption Spectra. The UV–visible spectra of the pseudooctahedral and pseudo-TP complexes were investigated to determine the effect of the geometries on the electronic structure of the complexes. The absorption spectra of the complexes $[Ti(BCT)]^{2-}$, $[Ti(eta)_3]^{2-}$, $[V(BCT)]^{2-}$, $[V(eta)_3]^{2-}$, $[Fe(BCT)]^{3-}$, $[Fe(BCTPT)]^{3-}$, and $[Fe(eta)_3]^{3-}$ in aqueous solution are presented in Figure 7.

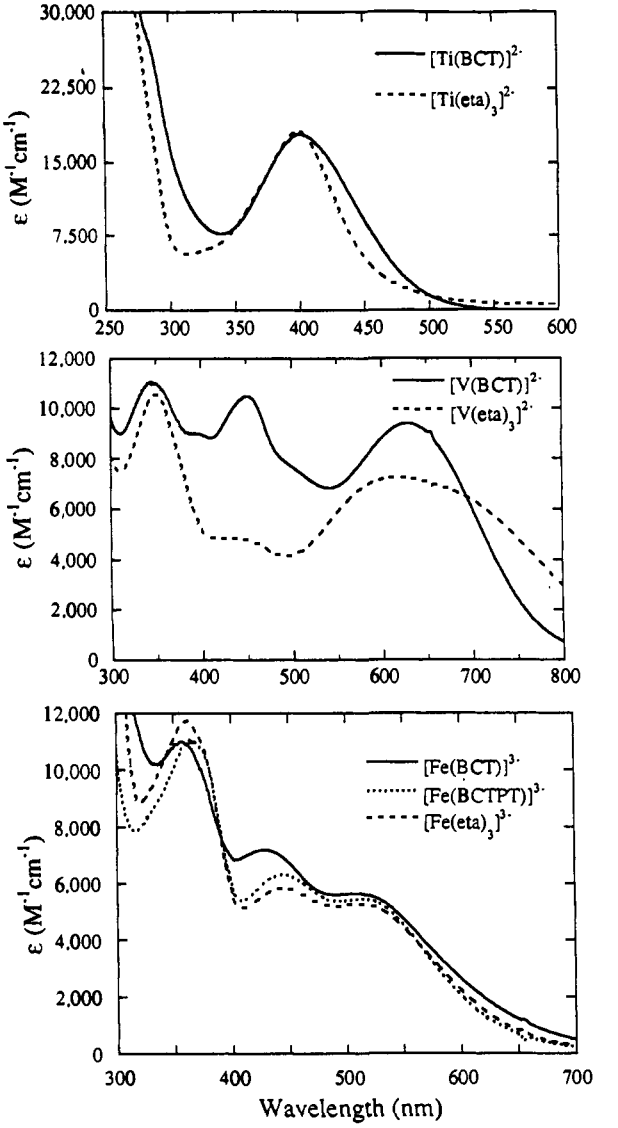

Figure 7. UV–visible spectra for the Ti^{IV} (top), V^{IV} (middle), and Fe^{III} (bottom) complexes in this study (H_2O, pH 7).

The $[V(eta)_3]^{2-}$ complex has been structurally characterized and is pseudooctahedral (α = 37°).[20] Although the crystal structure of $[Ti(eta)_3]^{2-}$ has not been obtained, a pseudooctahedral geometry is expected based on other catechol complexes. The Al and Ga complexes lack metal based UV–visible transitions and will not be discussed here. We have previously elucidated the electronic structure of $[Fe(eta)_3]^{3-}$ (and $[Fe(catechol)_3]^{3-}$) using single-crystal polarized absorption and magnetic circular dichroism spectroscopies,[23] and the results of that study provide a framework from which the source of the differences in the spectra of the Fe^{III} complexes may be identified. In the iron(III) complexes the band at ≈360 nm arises from a ligand (π–π^*) transition, whereas the transitions at lower energy are ligand to metal charge-transfer (LMCT) transitions. A comparison of the spectra of $[Fe(BCT)]^{3-}$, $[Fe(BCTPT)]^{3-}$, and $[Fe(eta)_3]^{3-}$ in the LMCT region (Figure 7) shows that the lower energy band at 512 nm varies only slightly, whereas the higher energy LMCT band is shifted and significantly more intense in $[Fe(BCT)]^{3-}$. Both of these absorptions are assigned in $[Fe(eta)_3]^{3-}$ as ligand-π to metal-d transitions, each arising from a different ligand orbital and terminating on the same metal d orbital. Specifically, the ligand and metal orbitals involved in these two transitions (I and II) are shown in Figure 8. The metal e^a set (the notation is the same as in Figure 3) contains the

(22) Shannon, R. D. *Acta Crystallogr. Sect. A* **1976**, *A32*, 751.

(23) Karpishin, T. B.; Gebhard, M. S.; Solomon, E. I.; Raymond, K. N. *J. Am. Chem. Soc.* **1991**, *113*, 2977.

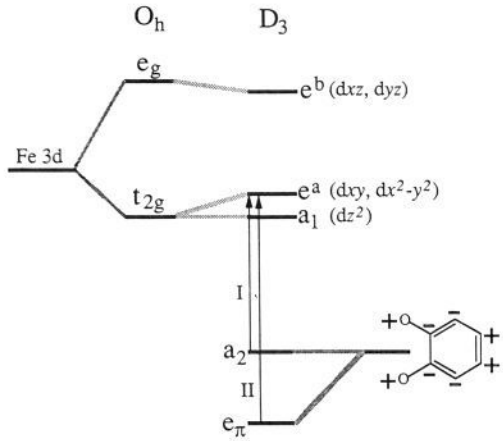

Figure 8. Molecular orbital scheme for the observed LMCT transitions in Fe^{III} tris(catecholates), see ref 23.

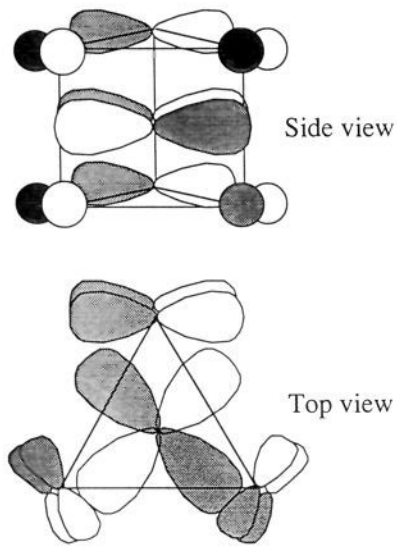

Figure 9. Illustration of the π-bonding interaction which is maximized in a trigonal prism. Only the out of plane pπ orbitals of the catecholate O atoms and the symmetry-matched metal d-orbitals are shown. The orientation is with respect to the 3-fold axis of D_{3h} symmetry.

d_{xy} and $d_{x^2-y^2}$ orbitals, which are degenerate and are in the plane perpendicular to the 3-fold axis.[24] The ligand a_2 orbital is nonbonding; in contrast, the ligand e_π orbital contributes to a π bonding molecular orbital. The energy difference between these orbitals, which correlates with the difference between I and II, is a measure of the π-bonding in these complexes.[23] Since band II is shifted by $\approx$900 cm^{-1} in $[Fe(BCT)]^{3-}$ relative to the pseudo-O_h complexes, a larger degree of π-bonding is indicated. The ligand MO and metal d orbital that are involved in transition II are illustrated in Figure 9. The π-overlap in this interaction is maximized in the trigonal prismatic geometry as drawn. As each bidentate group twists, increasing α, this overlap is reduced. Indeed, the larger extinction coefficient for transition II in $[Fe(BCT)]^{3-}$ compared to $[Fe(BCTPT)]^{3-}$ and $[Fe(eta)_3]^{3-}$ is consistent with a larger degree of π overlap.

In the spectra of the V^{IV} complexes (Figure 7), the band at $\approx$350 nm is ligand based, whereas the lower energy bands are all LMCT transitions.[25] It has been determined recently that the LMCT assignments for the Fe^{III} tris(catecholates) are also applicable to the V^{IV} tris(catecholates): the LMCT bands are ligand-π to metal-d transitions which are shifted by $\approx$4700 cm^{-1}

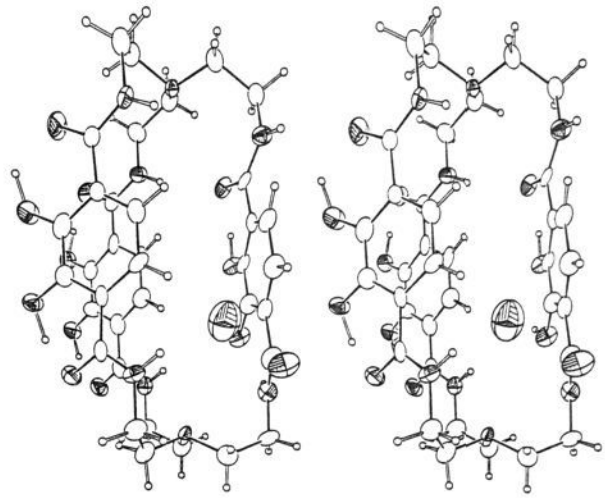

Figure 10. An ORTEP stereoview of H_6(bicappedTRENCAM)·H_2O.

to lower energy relative to the Fe^{III} complexes.[26] A similar increase in the extinction coefficients for these LMCT transitions in $[V(BCT)]^{2-}$ compared to $[V(eta)_3]^{2-}$ is again consistent with increased π overlap in the $[V(BCT)]^{2-}$ complex. In the Ti^{IV} complexes, the spectra are dominated by one very large LMCT transition at 400 nm[27] (which obscures the ligand π–π^* transition) that is equally intense in both the eta and BCT complexes (Figure 7). Clearly, the spectra of the Ti^{IV} complexes are significantly different from the V^{IV} and Fe^{III} complexes; no conclusions regarding π-bonding in the Ti complexes can be made.

VIII. π-Bonding Effects. We conclude from the spectroscopy of the Fe^{III} and V^{IV} complexes that *π-bonding* is the phenomenon responsible for the observed distortion toward trigonal prismatic geometry in the series of BCT complexes. In each of the Ti, V, and Fe complexes there are available d-orbitals for π-bonding that are filled in the case of Ga and not accessible in energy for Al. The ligand framework predilection for a trigonal prismatic geometry (vide infra) in conjuction with π-bonding stabilizes a pseudotrigonal prismatic arrangement of the six oxygen atoms in the case of the d-block metals. In the Al and Ga complexes this stabilization is lost. Consequently the coordination environment around the metal ions is determined primarily by repulsive interactions. To maximize the twist angle, the O atoms in turn must twist out of the catechol plane in the Al and Ga complexes.

The effects of π-bonding on the stereochemistry of six-coordinate complexes have been previously presented. Hoffmann and co-workers have performed theoretical calculations on the geometries of transition metal complexes (specifically varying between octahedral and TP) in which they concluded that π-bonding can lower the energy of the trigonal prism.[28] In addition, Comba and co-workers have investigated a series of hexaamine cage complexes.[18] They saw trend in twist angles that correlated with CFSE; however, with the structure of a V^{IV} complex where two of the ligating amines were deprotonated to imines, the twist angle was anomalously low (α = 18°). They suggested that π-bonding effects may be operative in that complex. It has also been proposed that strong π-bonding may contribute to the stabilization of the TP geometries seen in several tris(dithiolate) complexes,[4] which are close analogs of the catechol-based ligands described here. [It has been suggested by a referee that a relatively simple numerical calculation for the Fe^{III} tris(catecholate) complex would provide a more reliable basis for discussion of the bonding. On the contrary, the one Fenske–Hall molecular orbital calculation that has been published predicted the wrong ground state by approximately 100 kcal/mol. The description provided here well

(24) These d-orbitals differ from those usually derived from the t_{2g} set in O_h (i.e. d_{xy}, d_{yz}, and d_{xz}) because the principal axis (z) chosen is the 3-fold rather than the 4-fold (as is customary when operating in O_h symmetry).

(25) Cooper, S. R.; Koh, Y. B.; Raymond, K. N. *J. Am. Chem. Soc.* **1982**, *104*, 5092.

(26) Karpishin, T. B.; Dewey, T. M.; Raymond, K. N. *J. Am. Chem. Soc.*, in press.

(27) Borgias, B. A.; Cooper, S. R.; Koh, Y. B.; Raymond, K. N. *Inorg. Chem.* **1984**, *23*, 1009.

(28) Hoffmann, R.; Howell, J. M.; Rossi, A. R. *J. Am. Chem. Soc.* **1976**, *98*, 2484.

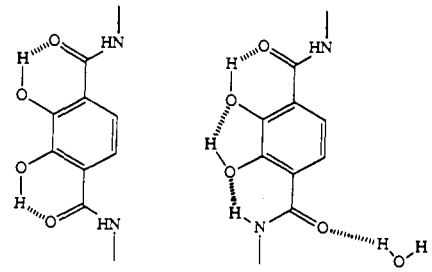

A B

Figure 11. The two types of H-bonding seen in the structure of H_6(bicappedTRENCAM)·H_2O.

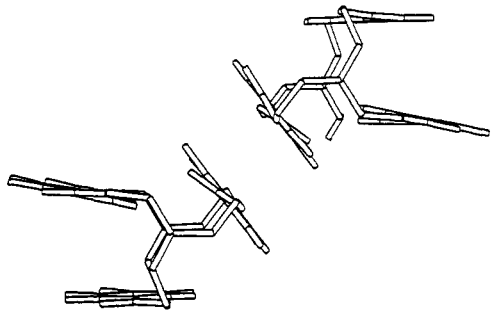

Figure 12. Diagram showing the intra- and intermolecular π-stacking in the structure of H_6(BCT) as viewed down the apical nitrogen (N1–N2) vector.

matches the detailed spectroscopic and bonding analysis described for catechol iron complexes.[23]]

IX. Structure of the Ligand, H_6(BCT). The crystal of the free ligand, H_6(BCT), has also been determined and an ORTEP stereoview is shown in Figure 10. Although a previous solution thermodynamic study of bicappedTRENCAM suggested that the H_6L species would be protonated at both apical nitrogens and deprotonated at two catechol oxygens (i.e., zwitterionic),[13] in the solid-state structure the six protons in H_6(BCT) (Figure 10) reside on the six catechol oxygens (see Crystallography section). One water molecule crystallizes in the unit cell per H_6(BCT) molecule, and this has a profound effect on the intramolecular H-bonding seen in the structure. The two terephthalamide groups at the left of Figure 10 show the same intramolecular H-bonding, in which the hydroxyl hydrogens are bound to the adjacent carbonyl oxygens (depicted as **A** in Figure 11). This type of H-bonding has been seen in other structures of protonated terephthalamide ligands.[21] The water molecule is H-bonded to the carbonyl oxygen at the bottom right of Figure 10 (O–O = 2.74 Å) which causes that amide group to H-bond in an alternate fashion (depicted as **B** in Figure 11).

An additional significant aspect of this crystal structure is the extensive π-stacking between the terephthalamide groups. In Figure 12, both the intramolecular and intermolecular stacking can be seen. The closest C–C contacts between the planes are 3.5 and 3.4 Å for the intra- and intermolecular stacking, respectively.

The impetus for the determination of the structure of H_6(BCT) was to examine the "relaxed" conformation of the ligand and thus investigate the extent of strain upon coordination to a metal. From Figures 10 and 12, the preferred "trigonal prismatic" geometry of the ligand is evident. That is, the ligand adopts a conformation in which there is no inherent twist in the terephthalamide arms. If a least squares plane is defined by the three C atoms bound to each apical nitrogen (on top and bottom), two reference points are developed from which to measure the twist of the catechol groups. The dihedral angles between the catechol (C_6) planes and these planes provide the effective twist of the binding subunits (Figure 13). If there is no effective twist in the binding subunits, the dihedral angles would all be 90°. In the structure of H_6(BCT), the average of these six dihedral angles is 92 (1)°. In the titanium, vanadium, and both iron BCT structures the average dihedral

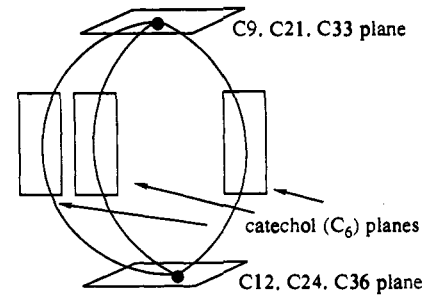

Figure 13. Illustration of the planes used to determine the effective twist of the catechol groups.

angle ranges slightly from 92–94°. However, in $[Ga(BCT)]^{3-}$ the average is 102 (1)°, and in $[Al(BCT)]^{3-}$ the average is 106 (1)°. The molecule is thus strained more from its "relaxed" conformation as the twist angle increases. From further analysis of the structure of H_6(BCT) however, it is apparent that even coordination to a metal in a TP fashion results in some strain in the ligand backbone. Starting with the crystallographically defined ligand geometry, simple rotation of the catecholate groups to an appropriate geometry for metal complexation results in significant van der Waals interactions between the catecholate oxygens.[29] The ligand framework must therefore *bow outwards* to expand the macrocyclic cavity and allow coordination to a metal. This effect can be observed in the shortening of the apical N–N distance (N1 to N2 in Figure 4) for the metal complexes relative to the free ligand (Table I). The N–N distance in H_6(BCT) is 10.47 Å. In the prismatic structure, $Na_3[Fe(BCT)]$, there is the least amount of this "expansion strain" with the N–N distance of 10.03 Å. However, as the twist angle increases, the ligand framework also must twist, and the N–N distance shortens to 9.68 Å in $[Al(BCT)]^{3-}$ (Table I).

X. Metal Ion Encapsulation. From the structures of H_6(BCT), $Na_3[Fe(BCT)]$, and $K_3[Fe(BCT)]$, it is clear that the initial design of the H_6(BCT) ligand for the complexation of iron[16] was off target in that the ligand is better suited for the encapsulation of metal ions smaller than Fe^{III}. Thus, it may be possible to make the BCT complexes of very small highly charged ions such as P^V and Si^{IV} (tris(catecholate) complexes of P^V and Si^{IV} are known[30,31]), whereas most other d-block metals may be too large to fit in the BCT cavity.

The ligand BCTPT would appear to generate a cavity size more appropriate for encapsulation of the ferric ion. The severe disorder in the TPT caps of $[Fe(BCTPT)]^{3-}$ (see Crystallography section) indicates, however, that the propyl bridge is too flexible and that the cavity is *too large* for Fe^{III}. The mixed-capped ligand bicapped (TPTTRENCAM), which has been previously prepared[13], may have the best cavity size for Fe^{III}.

XI. Structural Differences between $Na_3[Fe(BCT)]$ and $K_3[Fe(BCT)]$. The differences between the K^+ and Na^+ salts of the Fe complex are significant and must be rationalized as arising from crystal packing forces. Since both perfect and pseudotrigonal prismatic geometries are observed for $[Fe(BCT)]^{3-}$, a minimal energy difference between the geometries is suggested. Structural comparisons of the iron position in these two structures, relative to nonstrained structures such as $[Fe(eta)_3]^{3-}$, indicate that the Na^+ structure is of higher energy. The stabilization of the Na^+ structure most likely results from the 36 water molecules in the unit cell.[13] Hexagonal channels of hydrogen bonded water molecules have been shown to affect the structures of Al and Ga complexes of 3-hydroxy-2-methyl-4-pyridinone.[32]

Conclusions

This paper has reported: the syntheses and structures of five metal complexes of the macrobicyclic ligand bicappedTRENCAM

(29) Molecule Editor (CAChe), Version 2.8; CAChe Scientific, Inc.: 1991.
(30) Allcock, H. R.; Bissel, E. C. *J. Am. Chem. Soc.* **1973**, *95*, 3154.
(31) Flynn, J. J.; Boer, F. P. *J. Am. Chem. Soc.* **1969**, *91*, 5756.
(32) Nelson, W. O.; Karpishin, T. B.; Rettig, S. J.; Orvig, C. *Inorg. Chem.* **1988**, *27*, 1045.

(BCT), the synthesis and structure of the Fe^{III} complex of a larger macrobicycle (bicappedTPTCAM), and the structure of the comparison tris(bidentate) complex, $[Fe(eta)_3]^{3-}$. In addition, a synthetically expedient method to large quantities of the macrobicyclic ligands has been developed. The stereochemistries of $[Ti(BCT)]^{2-}$, $[V(BCT)]^{2-}$, and $[Fe(BCT)]^{3-}$ are all found to be very close to trigonal prismatic, whereas the complexes $[Al(BCT)]^{3-}$ and $[Ga(BCT)]^{3-}$ more closely resemble other tris(catecholate) structures in being pseudooctahedral. Spectroscopic evidence suggests that π-bonding within the d-block metal complexes stabilizes the trigonal prismatic geometry within the constraints of the macrobicyclic ligand. The solid-state structure of the free ligand, $H_6(BCT)$, indicates that the ligand is predisposed to trigonal prismatic coordination and that it becomes more strained in the pseudooctahedral complexes. The structure of the complex anion in $K_3[Fe(BCT)]$ is shown to be slightly different than in the previously determined structure of $Na_3[Fe(BCT)]$, and crystal packing forces from lattice water molecules are concluded to be the source of the differences.

Experimental Section

Physical Measurements. ^1H NMR spectra were measured at 298 K on a Bruker AM-500 or AM-400 spectrometer. When the spectra were recorded in D_2O, they were referenced to 3-(trimethylsilyl)propionic-*2,2,3,3-d*$_4$ acid, sodium salt at $\delta = 0.00$ ppm. Absorption spectra were recorded on an HP 8450 UV–visible diode array spectrophotometer. Microanalyses were performed by the Analytical Services Laboratory, College of Chemistry, University of California, Berkeley. Analyses that were within 0.4% of the calculated were considered acceptable. FAB mass spectra were performed by the Mass Spectrometry Laboratory, College of Chemistry, University of California, Berkeley.

Preparation of Compounds. All manipulations and operations were performed under Ar or N_2 with dried solvents although most of the metal complexes showed no tendency to oxidize when exposed to oxygen over short periods of time. TREN was distilled from sodium spheres. $CHCl_3$ was distilled from 4 Å sieves. H_2(eta) was synthesized according to the published procedure.[33] TPT was prepared from tris(2-cyanoethylamine)[34] according to the published procedure.[35] All other compounds used were of reagent grade and were not further purified. All of the metal complexes are soluble in H_2O, MeOH, and DMSO.

Ligand Syntheses (See Scheme I). **2,3-Dimethoxyterephthalic Acid Chloride**[36] **(B).** Vacuum dried 2,3-dimethoxyterephthalic acid[17] (**A**, 26.4 g, 119 mmol, 1 equiv) was dissolved in ~100 mL of dry, refluxing dioxane under argon. The solvent was removed under vacuum, and the dried solid was redissolved in ~250 mL of dry dioxane with heating. After cooling the solution, 45 mL of $SOCl_2$ (undistilled) was added, and the solution was refluxed for 4 h under an argon flow. The volatiles were removed under vacuum with gentle heating to give a pale yellow oil. This compound was used without further purification.

2,3-Dimethoxyterephthalic Acid Bis(2-mercaptothiazolide) (C). A 60% oil suspension of NaH (10.56 g, 264 mmol, 2.2 equiv) was washed with hexanes (2×) and suspended in 250 mL of dry THF. An equimolar amount of 2-mercaptothiazoline (31.47 g, 264 mmol, 2.2 equiv) was dissolved in 150 mL of THF and transferred slowly via cannula to the NaH suspension. After hydrogen evolution had ceased, the solution was filtered with a course glass frit directly into a THF solution (~100 mL) of the pale yellow diacid chloride (**B**). The reaction mixture immediately turned cloudy yellow and eventually to an off orange color after 8 h at room temperature. The THF was evaporated, and the yellowish-orange solid was suspended in 700 mL of CH_2Cl_2. The solution was washed with 0.1 M NaOH (2×) and dried over $MgSO_4$. The CH_2Cl_2 solution was reduced to 30 mL and cooled to −20 °C for 1 h. The crystalline product was collected in two crops to give 34.5 g (69%) which was used without further purification: ^1H NMR ($CDCl_3$) δ 3.40 (t, CH_2, 4 H), 3.87 (s, CH_3, 6 H), 4.63 (t, CH_2, 4 H), 7.05 (s, ArH, 2 H).

Recovery of Unreacted A. The basic water washings of the above reaction were combined, and 100 mL of 1 M NaOH was added. The solution was brought to reflux for 2 h, and after cooling, the reddish solution acidified with concentrated HCl to pH 1. The volume was reduced to 400 mL, and after standing at room temperature for 2 days, 4.5 g of yellowish needles crystallized. Recrystallization of the yellow needles in 100 mL water gave 3.5 g of pure **A**.

Compound D (Scheme I). In a 2-L, round-bottomed flask was dissolved **C** (32.0 g, 74.7 mmol) in 1 L of CH_2Cl_2. A solution of TREN (1.00 mL, 6.68 mmol) in 250 mL of CH_2Cl_2 was added over 36 h to the stirring thiazolide solution. The solution was reduced in volume to 500 mL, extracted with 0.1 M KOH, dried ($MgSO_4$), and further reduced in volume to 200 mL to precipitate most of the excess **C**. The precipitate was collected, and the filtrate was chromatographed (SiO_2; 1–3% MeOH/CH_2Cl_2). At 3% MeOH, the product elutes as one broad yellow band (R_f 0.50, 5% MeOH/CH_2Cl_2). The solvent was removed to yield a yellow crystalline material (4.83 g, 67% based on TREN) which decomposes with prolonged exposure to air. It is used immediately or stored under N_2: ^1H NMR ($CDCl_3$) δ 2.89 (t, NCH_2CH$_2$, 6 H), 3.44 (t, CH_2-thiazoline, 6 H), 3.61 (qrt, CH_2NH, 6 H), 3.86 (s, OCH_3, 9 H), 3.92 (s, OCH_3, 9 H), 4.65 (t, CH_2-thiazoline, 6 H), 7.09 (d, ArH, 3 H), 7.72 (d, ArH, 3 H), 8.14 (t, NH, 3 H). Elemental Anal. for $C_{45}H_{51}N_7O_{12}S_6$: C, H, N.

Me_6(bicappedTRENCAM), Me_6BCT. A high dilution reaction apparatus was set up for simultaneous addition of two reagents, in which a 5-L, three-necked, round-bottomed flask was equipped with an overhead stirrer, a condenser, and two continuous addition pumps (FMI Lab Pump QG6, Fluid Metering Inc.). The two reagents, **D** (5.43 g, 5.05 mmol) and TREN (757 μL, 5.06 mmol), were each dissolved in 500 mL of $CHCl_3$. The main flask was charged with 3 L of $CHCl_3$, and all flasks were purged and maintained under a N_2 atmosphere. Addition took place into refluxing $CHCl_3$ at 5.5 mL/h. The reaction mixture was reduced to 500 mL, extracted with 0.1 M KOH, washed with brine, and dried ($MgSO_4$). The solution was then taken to dryness and applied to a flash column (SiO_2; 10% MeOH/$CHCl_2$; product R_f 0.30). The product was collected and dried (2.84 g, 65%). ^1H NMR ($CDCl_3$) δ 2.74 (t, NCH_2CH$_2$, 12 H), 3.62 (qrt, CH_2NH, 12 H), 3.84 (s, OMe, 18 H), 6.80 (s, ArH, 6 H), 7.58 (t, NH, 6 H). Elemental Anal. for $C_{42}H_{54}N_8O_{12}$: C, H, N.

H_6(bicappedTRENCAM)·2HBr, H_6BCT·2HBr. Me_6BCT (0.100 g) was dissolved in 30 mL of degassed $CHCl_3$ and taken to 0 °C at which time 1.00 mL of BBr_3 was added via syringe. The yellow suspension was stirred at room temperature under a blanket of Ar and equipped with a drying tube for 16 h. H_2O (10 mL) was added slowly, and the mixture was transferred to a 500-mL separatory funnel. An additional 200 mL of H_2O and 200 mL of $CHCl_3$ were added to facilitate separation. The aqueous layer (pH 1.5) contains the precipitated product. It was brought to a boil, filtered hot, and allowed to cool at 4 °C [NOTE: the ligand is insoluble in H_2O at room temperature from pH 0–4; however, it is soluble at 90 °C as the fully protonated species, i.e., at pH < 3]. Off-white needles (0.090 g, 80%) were collected, washed with acetone, and dried in vacuo. The product is very hygroscopic. ^1H NMR (DMSO-d_6) δ 2.83 (br s, CH_2N, 6 H), 3.57 (br s, CH_2N, 12 H), 3.76 (br s, CH_2N, 6 H), 6.81 (m, ArH, 6 H), 8.30 (br s, 3 H), 9.02 (br s, 3 H), 10.00 (br s, 1 H), 11.87 (br s, 2 H), 12.70 (br s, 3 H). Elemental Anal. for $C_{36}H_{42}N_8O_{12}$·2HBr·2H_2O: C, H, N.

H_6(bicappedTRENCAM), H_6BCT. To 100 mg of H_6BCT·2HBr in MeOH was added 2 equiv of NH_4OH as an aqueous solution. The solution was taken to dryness and washed with acetone to remove the NH_4Br. The white solid was collected and dried (80 mg, 96%): ^1H NMR (DMSO-d_6) δ 2.67 (br s, CH_2N, 12 H), 3.48 (br s, CH_2N, 12 H), 6.61 (s, ArH, 6 H), 8.01 (br s, NH, 6 H), 12.60 (br s, OH, 6 H).

Compound E (Scheme I). Over a 4-h period, a 100-mL solution of CH_2Cl_2 containing 0.25 mL of TPT (≈0.25 g, 1.33 mmol) was added to a 600-mL 2% MeOH/CH_2Cl_2 solution of compound **C** (10 g, 23.3 mmol, 18 equiv). The solution was allowed to stir for 1 h and then chromatographed through a flash SiO_2 column equilibrated with 2% MeOH/CH_2Cl_2. The column was washed with 250 mL of 2% MeOH/CH_2Cl_2 to remove traces of 2-mercaptothiazoline and the excess **C**. This process leaves the product and oligomerized products on the column, while allowing the reaction to be performed again with the excess **C**. The eluted solvent was combined and immediately subjected to a similar reaction cycle as described above maintaining 18 equiv of **C**. The entire process was repeated a third time for a total of 0.60 mL TPT added. The reaction solution was once again chromatographed through the same column, and the eluent washed twice with 0.1 M NaOH, dried ($MgSO_4$), and evaporated to give 5.2 g of pure **C** (this represents 88% recovery of the excess **C**). The flash column was developed with a MeOH gradient from 2–5% to give 2.65 g of compound **E** (75%). TLC (5% MeOH/CH_2Cl_2) R_f 0.50. The compound degrades slowly in solution but is stable when dried and stored under Ar: ^1H NMR ($CDCl_3$) δ 1.78 (br s, CH_2, 6 H), 2.55 (br s, CH_2N, 6 H), 3.44 (t, CH_2-thiazoline, 6 H), 3.52 (qrt, CH_2N, 6 H), 3.88 (s, OMe, 9 H), 3.90 (s, OMe, 9 H), 4.65 (t, CH_2-thiazoline, 6 H), 7.10 (d, ArH, 3 H), 7.73 (d, ArH, 3 H), 8.04 (t, NH, 3 H).

(33) Garrett, T. M.; Miller, P. W.; Raymond, K. N. *Inorg. Chem.* **1989**, *28*, 128.
(34) Dietrich, B.; Hosseini, M. W.; Lehn, J.-M.; Sessions, R. B. *Helv. Chim. Acta* **1985**, *68*, 289.
(35) Chin, J.; Banaszczyk, M.; Jubian, V.; Zou, X. *J. Am. Chem. Soc.* **1989**, *111*, 186.
(36) Stutte, P.; Kiggen, W.; Vögtle, F. *Tetrahedron* **1987**, *43*, 2065.

Me_6(bicappedTPTCAM), Me_6BCTPT. The same high dilution reaction apparatus used to make Me_6BCT was utilized to make the analogous TPT ligand using 0.96 g of compound **E** and 0.162 g of TPT. Flash chromatography of the crude product (after workup) using a MeOH gradient (2–6% MeOH/CH_2Cl_2) gave 0.32 g (39%) of a white solid: ^{1}H NMR ($CDCl_3$) δ 1.66 (t, CH_2, 12 H), 2.53 (t, CH_2N, 12 H), 3.45 (m, CH_2, 12 H), 3.63 (s, OMe, 18 H), 7.69 (s, ArH, 6 H), 8.20 (t, NH, 6 H).

H_6(bicappedTPTCAM)·2HBr, H_6BCTPT·2HBr. Under an Ar flow, 1.0 mL of BBr_3 (2.65 g; 10.6 mmol) was added to a 10-mL solution of Me_6BCTPT (0.15 g, 0.158 mmol). A white precipitate immediately formed which had to be broken up with a glass rod. The reaction was monitored by ^{1}H NMR and deemed complete after 4 days. The entire reaction mixture was quenched in water, heated to reflux, and cooled, and a beige solid was collected. The solid was dissolved in MeOH and evaporated to dryness multiple times. The product was dried under vacuum at 70 °C to give an off white solid (0.12 g, 74%): ^{1}H NMR (DMSO-d_6) δ 1.85 (br s, CH_2, 12 H), 2.99 (br s, CH_2N, 12 H), 3.48 (br s, CH_2N, 12 H), 7.24 (s, ArH, 6 H), 8.89 (t, NH, 5 H), 9.80 (t, NH, 1 H), 12.83 (s, OH, 6 H).

Metal Complex Syntheses. [Ga(acac)$_3$]. To an aqueous solution (40 mL) of $GaCl_3$ (0.023 mmol) was added 7.22 g of 2,4-pentanedione (0.072 mmol). An additional 150 mL of H_2O was added to solubilize the 2,4-pentanedione. The pH was adjusted to 7.3 with 4 M NH_4OH. The yellow precipitate was collected and dried (7.3 g, 87%). Large yellow crystals are obtained from evaporation of acetone/MeOH solutions: ^{1}H NMR ($CDCl_3$) δ 2.00 (s, CH_3, 18 H), 5.40 (s, CH, 3 H). Elemental Anal. for $GaC_{15}H_{21}O_6$: C, H.

K$_3$[Al(BCT)]. To 100 mg of H_6BCT·2HBr (0.106 mmol) in MeOH was added Al(acac)$_3$ (0.035 g, 0.108 mmol). An aqueous solution of KOH was then added dropwise (5.39 mL, 0.0986 M, 0.531 mmol) and the solution turned gold in color. The yellow solid obtained after rotary evaporation was applied to a Sephadex LH-20 column in MeOH. The yellow complex eluted as a single band and 0.095 g were obtained (98%): MS (FAB$^+$) *m/e* 917 (K_3[Al(BCT)]H$^+$); ^{1}H NMR (D_2O) δ 2.72 (br m, CH_2N, 12 H), 3.58 (br m, CH_2NH, 12 H), 6.85 (s, ArH, 6 H). Elemental Anal. for $K_3AlC_{36}H_{36}N_8O_{12}$: C, H, N.

K$_2$[Ti(BCT)]. To a solution of 75 mg of H_6BCT·2HBr (0.080 mmol) in 50 mL of degassed MeOH was added an ethanolic solution of KOH (609 μL, 0.50 M, 0.304 mmol, 3.8 equiv). $[TiO(acac)_2]_2$ (0.021 g, 0.040 mmol) was added as a methanol suspension, and the color immediately turned deep orange. The solution was stirred for 2 h, and the solid obtained after rotary evaporation was applied to a Sephadex LH-20 column in MeOH. The deep orange band was separated from a canary yellow leading band on the column, and 35 mg was obtained (49%): ^{1}H NMR (D_2O) δ 2.86 (br m, NCH_2, 12 H), 3.72 (br m, CH_2NH, 12 H), 6.98 (s, ArH, 6 H), 10.66 (br s, NH, 6 H); complete exchange of the amide protons requires ≈1 h; UV–vis (H_2O, pH 7, λ (nm), ϵ (M^{-1} cm^{-1})) 400, 18 000. Elemental Anal. for $K_2TiC_{36}H_{36}N_8O_{12}\cdot 3H_2O$: C, H, N.

K$_2$[Ti(eta)$_3$]. Synthesized and purified in a similar fashion to K_2[Ti(BCT)] using 1.9 equiv of KOH: ^{1}H NMR (DMSO-d_6) δ 1.09 (t, CH_3, 18 H), 3.25 (qrt, CH_2NH, 12 H), 7.10 (s, ArH, 6 H), 8.96 (t, NH, 6 H); UV–vis (H_2O, pH 7, λ (nm), ϵ (M^{-1} cm^{-1})) 400, 18 200. Elemental Anal. for $K_2TiC_{36}H_{42}N_6O_{12}\cdot 3H_2O$: C, H, N.

K$_2$[V(BCT)]. To a solution of 75 mg of H_6BCT·2HBr (0.079 mmol) in 50 mL of degassed MeOH was added an ethanolic solution of KOH (634 μL, 0.50 M, 0.317 mmol). The solution immediately turned yellow and all of the ligand dissolved. $VO(acac)_2$ (0.021 g, 0.079 mmol) was then added and the solution turned forest green in color. A drop of 1% HBr was added and after 2 min, the solution turned a much deeper green. Based on the UV–visible spectra of vanadium catecholate complexes, the deep green color is due to the tris(catecholate) complex, $[V(BCT)]^{2-}$, whereas the paler color is due to a vanadyl complex, presumably $[VO(BCTH_2)]^{2-}$, which would be favored at higher pH.[25] The solution was heated at reflux overnight, filtered, and taken to dryness. The solid was then applied to a Sephadex LH-20 column in MeOH, and the dark green product was separated from a small amount of the pale green complex. UV-vis (H_2O, pH 7, λ (nm), ϵ (M^{-1} cm^{-1})) 450, 10 500; 630, 9400. Elemental Anal. for $K_2VC_{36}H_{36}N_8O_{12}\cdot H_2O$: C, H, N.

K$_2$[V(eta)$_3$]. Synthesized and purified in a similar fashion to K_2[V(BCT)] using 1.9 equiv of KOH: UV–vis (H_2O, pH 7, λ (nm), ϵ (M^{-1} cm^{-1})) 436, 4900; 616, 7200. Elemental Anal. for $K_2VC_{36}H_{42}N_6O_{12}\cdot 2H_2O$: C, H, N.

K$_3$[Fe(BCT)]. To a solution of 100 mg of H_6BCT·2HBr (0.106 mmol) in 40 mL of degassed MeOH was added an ethanolic solution of KOH (1.048 mL, 0.50 M, 0.524 mmol). $Fe(acac)_3$ (0.037 g, 0.105 mmol) was added, and the solution turned deep red. The solution was stirred for 30 min, and the solid obtained after rotary evaporation was applied to a Sephadex LH-20 column in MeOH. The red complex eluted as a single band and 90 mg was obtained (90%): UV–vis (H_2O, pH 7.4, λ (nm), ϵ (M^{-1} cm^{-1})) 428, 7200; 506, 5600. Elemental Anal. for $K_3FeC_{36}H_{36}N_8O_{12}\cdot 3H_2O$: C, H, N.

K$_3$[Fe(eta)$_3$]. Synthesized and purified in a similar fashion to K_3[Fe(BCT)] using exactly 3 equiv of KOH: UV–vis (H_2O, pH 7.4, λ (nm), ϵ (M^{-1} cm^{-1})) 444, 5800; 512, 5300. Elemental Anal. for $K_3FeC_{36}H_{42}N_6O_{12}\cdot 3H_2O$: C, H, N.

K$_3$[Ga(BCT)]. To a solution of 51 mg of H_6BCT·2HBr (0.054 mmol) in 50 mL of degassed MeOH was added an ethanolic solution of KOH (540 μL, 0.50 M, 0.270 mmol). The addition of Ga(acac)$_3$ (0.020 g, 0.054 mmol) did not effect a color change. The solution was stirred for 30 min, and the solid obtained after rotary evaporation was applied to a Sephadex LH-20 column in MeOH. The pale yellow complex eluted as a single band, and 45 mg was obtained (87%): MS (FAB$^-$) *m/e* 843 $[Ga(BCT)H_2]^-$; ^{1}H NMR (D_2O), δ 2.84 (br m, CH_2, 12 H), 3.70 (br m, CH_2, 12 H), 6.95 (s, ArH, 6 H). Elemental Anal. for $K_3GaC_{36}H_{36}N_8O_{12}$: C, H, N.

K$_3$[Fe(BCTPT)]. Synthesized and purified in a similar fashion to K_3[Fe(BCT)] using H_6BCTPT·2HBr and 5 equiv of KOH: UV–vis (H_2O, pH 7.4, λ (nm), ϵ (M^{-1} cm^{-1})) 446, 6300; 512, 5400. Elemental Anal. for $K_3FeC_{42}H_{54}N_8O_{12}\cdot 3H_2O$: C, H, N.

Crystallography. General Methods. For each of the crystal structures presented a low-temperature data set was collected as described, since crystals of these complexes tend to be very susceptible to solvent loss. A suitable crystal was mounted on the end of a glass capillary with Paratone oil (Exxon) and placed under a cold nitrogen stream on an Enraf-Nonius CAD-4 automatic diffractometer. Unit cell parameters and an orientation matrix were typically obtained from 24 machine-centered reflections with 2θ near 24°. Data collection and crystal parameters for the eight structures are provided in Table III. Three check reflections monitored every hour of X-ray exposure were used to determine if there was significant crystal decay. A linear decay correction (5.6%) was deemed necessary only for the K_3[Fe(eta)$_3$] data set. An empirical absorption correction was applied to the following data sets based on ψ-scan data: K_3[Al(BCT)], from 0.91 to 0.96 on I: K_2[Ti(BCT)], from 0.82 to 1.00 on I; K_3[Fe(BCTPT)], from 0.95 to 1.00 on I; K_3[Ga(BCT)], from 0.91 to 1.00 on I. The data were processed and the structures were refined using MolEN.[37] Atom scattering factors were taken from the tabulations of Cromer and Waber.[38] In each case, the systematically absent data were removed, and the structure was solved using the direct methods program SHELXS.[39] If all of the atoms were not located from the SHELXS output, the remaining atoms were found by cycles of Fourier analysis and least squares refinement or, in the case of H atoms, put in at idealized positions.[40] Specific details for each of the crystal structures[41] are found in the following sections. All of the BCT structures have consistent atomic numbering schemes as shown in Figure 4; the atomic numbering schemes for $[Fe(BCTPT)]^{3-}$ and $[Fe(eta)_3]^{3-}$ are provided in the supplementary material. ORTEP views of the eight structures, tables of positional parameters, bond lengths, bond angles, and anisotropic thermal factors are found in the supplementary material.

K$_3$[Al(BCT)]·6acetone·2H$_2$O. X-ray quality crystals were obtained by vapor diffusion of acetone into an aqueous solution of K_3[Al(BCT)]. All of the non-hydrogen atoms except those of the solvent were assigned anisotropic thermal parameters; however, those for two of the C atoms in the ligand became nonpositive definite. Therefore, only the K and Al atoms were refined with anisotropic thermal parameters. The TREN backbone on one side of the molecule was found to be disordered over two positions. The atoms C12, C24, and C36 were set at 60% occupancy, whereas C12′, C24′, and C36′ were set at 40%. This disorder is due to facile twisting of the TREN caps. Four of the six amide protons were located by difference Fourier maps, with the six protons included at calculated positions (0.95 Å from their parent atoms) for least squares refinements. Final refinement converged at $R = 7.63\%$. The space group is $P2_12_12_1$ ($Z = 4$) requiring, in the absence of inversion twinning, only one of the trischelate isomers to be in the unit cell. Refinement of the enantiomorphic structure converged to 7.68%, indicating that the anomalous dispersion due to the Al atoms is too small to assign unequivocally the isomer in this structure.

K$_2$[Ti(BCT)]·4DMF·1.5H$_2$O. X-ray quality crystals were obtained by layering Et_2O onto a solution of K_2[Ti(BCT)] in wet DMF. After ≈75% of the data set was collected, the crystal fractured under the cold stream.

(37) Molen Structure Determination System; Enraf-Nonius Delft: 1991.
(38) Cromer, D. T.; Waber, J. T. *International Tables for X-ray Crystallography*; Kynoch Press: Birmingham, England, 1974; Vol. IV.
(39) Sheldrick, G. *Crystallographic Computing 3*; Oxford University Press: 1985; pp 175–189.
(40) Allen, F. H.; Kennard, O.; Watson, D. G.; Brammer, L.; Orpen, A. G.; Taylor, R. *J. Chem. Soc., Perkin Trans. II* **1987**, S1.
(41) See the paragraph at the end of this manuscript regarding supplementary material.

However the structure was solved and refined with the data that had been obtained. In this structure, the TREN backbone was found to be disordered on both sides of the molecule. On the N1 side, the occupancy was set at 65/35 for (C9,C21,C33)/(C9′,C21′,C33′); on the N2 side, the occupancy was set at 75/25 for (C12,C24,C36)/(C12′,C24′,C36′). All of the six amide protons of the $[Ti(BCT)]^{2-}$ anion were located by a difference Fourier map; however, they were included at calculated positions (0.95 Å from their parent atoms) for least squares refinements. All non-hydrogen atoms, except the disordered carbons, were refined anisotropically.

K_2[V(BCT)]·4DMF·1.5H_2O. X-ray quality crystals were grown by layering Et_2O onto a solution of $K_2[V(BCT)]$ in wet DMF. Again the TREN backbone on both sides of the molecule was found to be disordered. On the N1 side, the occupancy was set at 65/35 for (C9,C21,C33)/(C9′,C21′,C33′); on the N2 side, the occupancy was set at 85/15 for (C12,C24,C36)/(C12′,C24′,C36′). The water oxygens are O17 (occupancy, 1.0) and O18 (occupancy, 0.5). One DMF molecule (O14, N10, C40, C41, and C42) was found to be disordered; the C=O portion (O14 and C40) over two positions and the $N(Me)_2$ portion (N10, C41, C42) over three positions. All of the six amide protons of the $[V(BCT)]^{2-}$ anion were located by a difference Fourier map; however, they were included at calculated positions (0.95 Å from their parent atoms) for least squares refinements. All non-hydrogen atoms in the structure, with exception of the disordered DMF molecule, were refined anisotropically.

K_3[Fe(BCT)]·6DMF·H_2O. X-ray quality crystals were grown by layering Et_2O onto a solution of $K_3[Fe(BCT)]$ in wet DMF. The C=O portion (C13S and O6S) of one DMF molecule was disordered over two positions. The 36 protons in the $[Fe(BCT)]^{3-}$ anion were included at calculated positions (0.95 Å from their parent atoms) for structure factor calculations but were not refined. All non-hydrogen atoms in the structure, with exception of the disordered DMF atoms, were refined anisotropically.

K_3[Ga(BCT)]·6DMF·H_2O. X-ray quality crystals were grown by layering Et_2O onto a solution of $K_3[Ga(BCT)]$ in wet DMF. Four of the six DMF molecules were found to be disordered. The 36 protons in the $[Ga(BCT)]^{3-}$ anion were included at calculated positions (0.95 Å from their parent atoms) for structure factor calculations but were not refined. All non-hydrogen atoms in the structure, with exception of the disordered DMF atoms, were refined anisotropically.

K_3[Fe(BCTPT)]·4DMF·0.5H_2O. X-ray quality crystals were grown by layering Et_2O onto a solution of $K_3[Fe(BCTPT)]$ in wet DMF. The TPT backbone was found to be disordered at several positions. One of the apical nitrogens (N1) was disordered over two positions (50/50) and three TPT carbons were disordered: C10 (over two positions, 50/50); C28 (over two positions, 60/40); C37 (over three positions, 50/25/25). In addition the NMe_2 portion of one of the DMF molecules was disordered over two positions 60/40 (N4S, C11S, and C12S). All of the six amide protons were located by a difference Fourier map; however, they were included at calculated positions (0.95 Å from their parent atoms) for structure factor calculations but were not refined. All non-hydrogen atoms in the structure, with exception of the disordered atoms, were refined anisotropically.

K_3[Fe(eta)$_3$]·3acetone·2ethanol. X-ray quality crystals were obtained by vapor diffusion of acetone into an ethanol solution of $K_3[Fe(eta)_3]$ over 2 days. The ethanol oxygens sit on 3-fold axes in the unit cell which results in 3-fold disorder around each of them. This, in addition to disorder in the acetone molecules, caused problems in the anisotropic refinement of the $[Fe(eta)_3]^{3-}$ anion. Therefore, only the Fe and K atoms were refined anisotropically. The position of the Fe atom on the 3-fold axis was taken as the origin ($Z = 0$).

H_6(BCT)·H_2O. X-ray quality crystals were obtained by layering Et_2O onto a solution of $H_6(BCT)$ in wet DMF. All of the catechol hydroxyl protons were located by difference Fourier maps and were included for the structure factor calculations at their located positions. The remaining 36 protons in the ligand structure were included at calculated positions (0.95 Å from their parent atoms) for structure factor calculations but were not refined. To effectively determine the positions of the six acidic protons in the ligand, the catechol hydroxyl protons were removed for the last cycle of least squares refinement and a final difference Fourier map generated. On this map six of the top eight peaks were located within 1.1 Å of the six catechol oxygens. The remaining two difference Fourier peaks were not located within bonding radius of any atoms in the unit cell. None of the top 40 difference Fourier peaks were located within bonding radius of the apical nitrogens. The protons of the water molecule were not included for struture factor calculations. All of the non-hydrogen atoms in the structure were refined anisotropically.

Acknowledgment. This research was supported by the National Institutes of Health Grants AI 11744 and DK 32999. T. D. P. Stack thanks the National Science Foundation for a postdoctoral fellowship (1988–1990, CHE-880911).

Supplementary Material Available: ORTEP views, crystal data, and tables of positional parameters, bond lengths, bond angles, and anisotropic thermal factors for the eight crystal structures (67 pages). Ordering information is given on any current masthead page.